



ELSEVIER

Comput. Methods Appl. Mech. Engrg. 181 (2000) 437–449

**Computer methods  
in applied  
mechanics and  
engineering**

www.elsevier.com/locate/cma

# Computational issues in the simulation of semiconductor quantum wires

A. Trellakis, U. Ravaioli \*

*Department of Electrical and Computer Engineering, Beckman Institute, University of Illinois, Urbana-Champaign, Urbana, IL 61801, USA*

Received 1 February 1998

---

## Abstract

This paper introduces the main numerical issues related to the simulation of electronic states in highly confined semiconductor systems. A typical example is the semiconductor quantum wire, where double size quantization confines carriers on the cross-section of a conduction channel. We introduce details of the numerical approach for the solution of the coupled Poisson/Schrödinger equation system that describe the quantum system and outline an original iteration approach that uses a predictor–corrector procedure for convergence of the outer iteration. The numerical approach is illustrated by a number of examples for quantum wire structures based on the GaAs/AlGaAs and the Si/SiO<sub>2</sub> material systems. The simulations for Si-based structures are interesting to understand the limit of scalability of traditional integrated devices in the plane transverse to the conduction channel. It is also shown that a quasi–monomode Si quantum wire is in principle possible at room temperature. © 2000 Elsevier Science S.A. All rights reserved.

---

## 1. Introduction

As the dimensions of electronic devices approach nanometer scale, quantum effects are expected to have an ever increasing influence on their electronic properties, until at some point these effects become essential for device operation. Consequently, there is considerable interest in the efficient numerical simulation of such structures, both for exploring new device architectures as well as for scaling of more traditional structures.

In this paper, we discuss the simulation of structures formed by double quantization, usually called quantum wires. Besides offering a way to probe the physics of transport in purely one-dimensional systems, the simulation of quantum wires is also interesting because it allows one to get an insight on the ultimate limits of device scalability in the plane transverse to a conduction channel. The goal of this paper is to describe some efficient computational methods for simulating electronic states in quantum wires, along with examples that are relevant for practical applications.

There are a number of approaches suitable for the realization of quantum wires, all of which employ an electric potential and/or material boundaries to doubly confine carriers along two direction while they can move freely along the third one. For example, in the device cross-sections depicted in Figs. 1 and 2 the potential energy step at GaAs–AlGaAs or Si–SiO<sub>2</sub> heterojunctions prevents electron movement across an interface boundary, while an applied electrostatic potential attracts the electrons into a “potential well” close to the interface and prevents them from escaping into the substrate. The combination of these two

---

\* Corresponding author. Tel.: +1 217 244 5765; fax: +1 217 244 4333.  
E-mail address: ravaioli@uiuc.edu (U. Ravaioli).

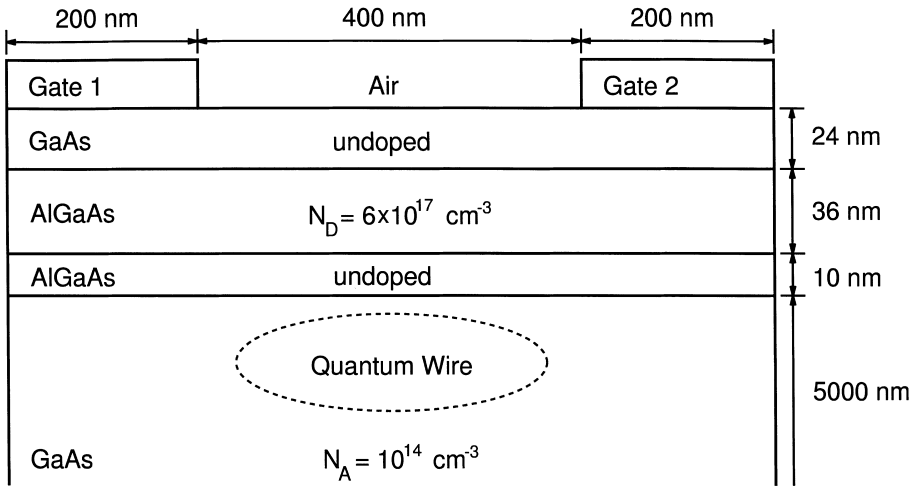


Fig. 1. A model GaAs–GaAlAs device structure used for numerical experiments.

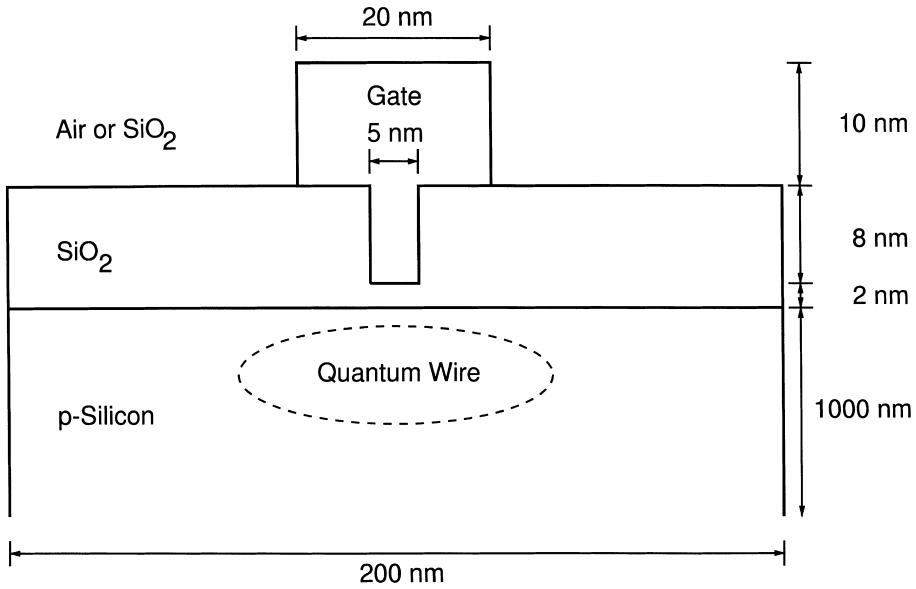


Fig. 2. A Si–SiO<sub>2</sub> based quantum device with a T-shaped gate. The acceptor concentration in the substrate is either  $N_A = 10^{10} \text{ cm}^{-3}$  or  $N_A = 10^{18} \text{ cm}^{-3}$ .

confining mechanisms generates size quantization in the cross-section, but a continuum of free states still remains for the third direction. Due to the similarity with guided propagation of electromagnetic waves, quantum wire structures are often referred to as “electron waveguides”.

The physical model used to describe the bound states in the cross-section of a quantum wire consists of the coupled system of Schrödinger’s and Poisson’s equations. Schrödinger’s equation in the effective mass approximation is defined as

$$-\frac{\hbar^2}{2} \nabla \cdot \left[ \frac{1}{m^*} \nabla \psi_l \right] + [V_h - e\phi + V_{xc}(n) - E_l] \psi_l = 0, \tag{1}$$

where  $\psi_l$  denotes the wavefunction belonging to energy level  $E_l$ ,  $\phi$  the electrostatic potential,  $V_h$  the heterojunction step potential,  $n$  the quantum electron density, and finally  $V_{xc}$  the exchange correlation potential in the local density approximation.  $m^*$  is the tensor describing the effective electron mass.

In GaAs the conduction band at the energy minimum consists of a single valley with approximately spherical symmetry. In silicon, the conduction band has six valleys (aligned in pairs along the principal axes of the momentum coordinates, or  $\langle 100 \rangle$  directions). The valleys are described by three different tensors for the effective mass. Therefore, in this case we have to solve Schrödinger’s equation three times and we obtain three different sets of eigenvalue ladders for the quantum states. In the calculations, we consider the typical interface orientation  $\langle 100 \rangle$ . The axis of the quantum wire is also assumed to be aligned along a direction of the  $\langle 100 \rangle$  family.

The electrostatic potential  $\phi$  is determined by a nonlinear Poisson equation

$$\nabla \cdot (\epsilon \nabla \phi) = -\rho(\phi), \tag{2}$$

$$\nabla \cdot (\epsilon \nabla \phi) = -e[-n + p(\phi) + N_D^+(\phi) - N_A^-(\phi)], \tag{3}$$

where  $\epsilon$  is the dielectric constant,  $e$  the unit electric charge,  $p$  the hole density, and  $N_D^+$  and  $N_A^-$  the ionized donor and acceptor concentrations. The latter three quantities depend on  $\phi$  as

$$p(\phi) = 2 \left( \frac{m_{dh} k_B T}{2\pi \hbar^2} \right)^{3/2} \mathcal{F}_{1/2} \left( \frac{-e\phi + V_h - E_G - E_F}{k_B T} \right), \tag{4}$$

$$N_D^+(\phi) = N_D \left[ 1 + g_D \exp \left( \frac{E_F + e\phi - V_h + E_d}{k_B T} \right) \right]^{-1}, \tag{5}$$

$$N_A^-(\phi) = N_A \left[ 1 + g_A \exp \left( \frac{-e\phi + V_h - E_G + E_a - E_F}{k_B T} \right) \right]^{-1}, \tag{6}$$

where  $N_D$  and  $N_A$  are the donor and acceptor concentrations,  $E_d$  and  $E_a$  the donor and acceptor atom ionization energies, and  $g_D$  and  $g_A$  their respective ground state level degeneracies.  $E_G$  is the band gap, and  $m_{dh}$  the density-of-state mass of the valence band.

The quantum electron density  $n$  occurring in both equations is obtained from the eigenpairs  $(E_l, \psi_l)$  of Schrödinger’s equation as

$$n = \sum_l N_l |\psi_l|^2, \tag{7}$$

where

$$N_l = g_V \left( \frac{2m_w k_B T}{\pi^2 \hbar^2} \right)^{1/2} \mathcal{F}_{-1/2} \left( \frac{E_F - E_l}{k_B T} \right) \tag{8}$$

denotes the occupancy of the eigenstate  $l$ ,  $g_V$  the number of equivalent conduction band valleys,  $m_w$  the electron mass along the wire axis,  $T$  the temperature,  $k_B$  Boltzmann’s constant,  $E_F$  the Fermi level, and  $\mathcal{F}_{-1/2}$  the complete Fermi–Dirac integral of order  $-1/2$ . For silicon-based structures the quantum electron density is determined by adding the three partial densities corresponding to the three nonequivalent valleys.

Poisson’s equation is nonlinear, because the carrier population and the density of ionized impurities in the substrate are included through a quasi-equilibrium classical density which depends self-consistently on the potential being solved for.

## 2. Solution of Poisson’s equation

The semiconductor structures that we consider here consist of material layers which lend themselves to discretization on rectangular grids. Although an unstructured grid could allow one to reduce the number of grid points even further, a rectangular grid is a very good trade-off for our applications, because of simplification of the algorithms and high efficiency of the solvers.

Poisson’s equation is discretized using standard box integration on a two-dimensional nonuniform rectangular grid. Box integration is able to handle any rectangular device geometry as long as the grid lines conform with all material boundaries. Also, discontinuities in the dielectric profile  $\epsilon$  are naturally included,

since this scheme conserves the electric flux. Additionally, we condense the mesh in correspondence of the confinement region of the quantum wire to achieve sufficient accuracy and efficiency. The discretization matrix is sparse and banded, with a sparsity structure identical to that obtained by discretizing a laplacian with a 5-point stencil (2 bands above and below the diagonal). Therefore, we may use a banded storage scheme to represent the matrix, which is computationally more efficient than using a general sparse storage method based on pointer chasing.

The sparsity, together with the large size of the discretization matrix (about  $10^4 \times 10^4$ ), demands the use of a sparse matrix solver, such as the preconditioned conjugate gradient algorithm [1]. The performance of this algorithm depends crucially on the choice of the preconditioner: as we see in Fig. 3, using the well-known incomplete Cholesky (no fill-in) preconditioning method [1] improves upon diagonal preconditioning by a factor of about 10. On the other hand, using the less-known Dupont–Kendall–Rachford preconditioner [2,3], which is similar in its structure to incomplete Cholesky preconditioning, we get another speed-up by a factor of almost 2 (see Table 1).

Poisson's equation for semiconductor device simulation is nonlinear with a form

$$\nabla \cdot (\epsilon \nabla \phi) + \rho(\phi) = 0. \quad (9)$$

Therefore, we use for Eq. (9) a Newton–Raphson iteration approach. Since the Jacobian of Eq. (9)

$$J(\phi) = \nabla \cdot (\epsilon \nabla) + \frac{\delta \rho}{\delta \phi}(\phi) \quad (10)$$

adds only a diagonal term  $\delta \rho / \delta \phi$  to the matrix obtained from discretizing the linear Poisson equation, we can directly use the preconditioned conjugate gradient algorithm mentioned above to invert  $J(\phi)$  within Newton's method. Here, the necessary positive definiteness of the Jacobian is not obvious, but follows from the physical fact the the charge density  $\rho(\phi)$  is monotonic in  $\phi$  and increases with increasing  $\phi$ .

Finally, we have to mention that the simulation requires a great number of high-accuracy evaluations of Fermi–Dirac integrals [4], since every time we calculate the charge density or its derivative during Newton–Raphson iteration, we have to evaluate two such integrals for each grid point. To avoid the large

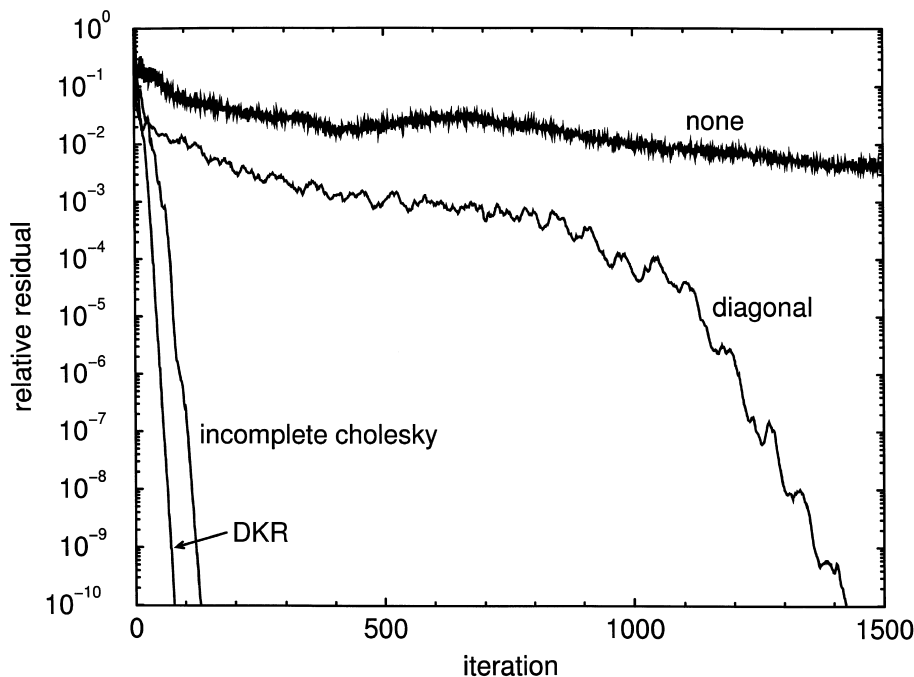


Fig. 3. The relative residual of the electrostatic potential  $\phi$  during the preconditioned conjugate gradient algorithm for the device shown in Fig. 1. Three different preconditioning techniques are shown.

Table 1

Number of iterations needed to achieve a relative residual of  $10^{-10}$  for different conjugate gradient preconditioners; the mesh size is  $88 \times 99$ , modeling the GaAs based structure (Fig. 1) at a gate bias of 1.3 V

Preconditioner	Number of iterations
None	6277
Diagonal	1424
Incomplete Cholesky (no fill-in)	130
Dupont–Kendall–Rachford (DKR)	77

computational costs involved here we use rational function approximations, which combine speed of execution with high accuracy [5,6].

### 3. Solution of Schrödinger's equation

Schrödinger's equation is discretized on the same grid as Poisson's equation, where a similar box-integration for nonuniform rectangular mesh is applied. This is a natural approach, since the variables and the operators in the two equations are affected similarly by the geometric variation in the structure and in our experience it is not necessary to further refine the grid for the quantum problem to improve accuracy. The use of a similar grid for both equations is also useful to avoid the cost of interpolation of quantities like the electron density  $n$  or the electrostatic potential  $\phi$  during the outer iteration for the coupled solution. The computational cost can be reduced if Schrödinger's equation is solved only on a sub-set of the original grid around the wire region where the quantum density is appreciable, while a semi-classical expression for the electron density

$$n(\phi) = 2 \left( \frac{m_{\text{dc}} k_{\text{B}} T}{2\pi \hbar^2} \right)^{3/2} \mathcal{F}_{1/2} \left( \frac{E_{\text{F}} + e\phi - V_{\text{h}}}{k_{\text{B}} T} \right) \quad (11)$$

is used everywhere else, with  $m_{\text{dc}}$  denoting the density-of-state mass of the conduction band.

After discretization we obtain a generalized symmetric eigenvalue problem, which can be easily transformed into the standard eigenvalue form, since the mass tensor is diagonal. An iterative approach that resolves only a limited sub-space of the eigenvalues is the only practical one here, since the matrix is large and sparse and involves a large number of eigenvalues (as many as the grid points). For our physical problem, we are exclusively interested in resolving the eigenvalues corresponding to confined states in the quantum well, with corresponding eigenstates representing the electronic wavefunctions. The desired range of solutions represents the lower portion of the eigenvalue spectrum. Our approach for the solution of the eigenvalue problem is based on Arnoldi's iteration method [1], which has the advantage of greater stability compared to Lanczos iteration. Since the eigenvalues tend to be condensed in a relatively small numerical range, a preconditioning strategy is necessary, so that in the preconditioned problem the eigenvalues are well separated in the desired range. We use a Chebyshev preconditioner [7,8] which is very suitable for the typical eigenvalue distribution in semiconductor quantum confinement problems.

General details on the numerical solution of eigenvalue problems and related issues are discussed in great depth in [9]. Here, we will only point out a few relevant issues. Arnoldi's method is based on iteration in a subspace (Krylov subspace), representing a projection of the total problem. The Krylov subspace is spanned by the so-called Krylov vectors, that correspond to eigenvectors of the problem. Each Krylov vector requires the same amount of memory for its storage as a desired eigenvector, however, the actual size of the Krylov subspace has to be two or three time larger than the size of the desired eigenvector space in order to achieve a sufficiently accurate solution, with a minimum of approximately 30 Krylov vectors in a practical algorithm. The time required for the computation of an eigenvector is proportional to the *square* of the total number of Krylov vectors in the chosen subspace [1]. Since the number of physically significant wavefunctions rapidly increases with temperature for a given quantum structure, simulation at room temperature is much more time and memory intensive than at a typical cryogenic temperature of 4.2 K.

An additional computational complication is that it is advantageous for convergence of the algorithm to preserve old Krylov vectors for the subsequent eigenvalue solutions. This is extremely demanding in terms of memory storage for silicon structures, since Schrödinger's equation needs to be solved independently at every step for each eigenvalue ladder (three in our case) which arises from the projection of the conduction band valleys onto the two-dimensional domain. Fortunately, numerical experiment shows that it is sufficient to preserve just one set of Krylov vectors between calls to the eigenvalue solver, without compromising the convergence speed. This behavior seems to indicate that an approximate Krylov space is sufficient for a successful initialization of the solver.

#### 4. Outer iteration

There is no obvious way to solve the two model equations simultaneously, since Poisson's equation is a boundary value problem and Schrödinger's equation is an eigenvalue problem. One has to rely on an iterative approach for solving this coupled system of equations [10,11]. However, due to the strong nonlinear coupling between both equations, a straightforward iteration is by itself not convergent. A standard approach for this kind of iteration is underrelaxation either in the electrostatic potential  $\phi$  or in the quantum electron density  $n$ . Unfortunately plain underrelaxation has a number of shortcomings. The outer iteration is controlled by the underrelaxation procedure only and therefore inherently unstable. As a result, we see strong oscillations of the total quantized charge  $\int n \, dx$  from one iteration step to the other, if the relaxation parameter  $\omega$  has been chosen too large. On the other hand, when  $\omega$  is too small the number of iteration steps necessary for convergence becomes very large. This is a problem, because  $\omega$  is not known in advance and needs to be dynamically readjusted during the course of the iteration using some empirical procedure.

To improve on this problem one should modify the iteration algorithm in a way that partially decouples both partial differential equations and damps the oscillations in the total electric charge. Improving upon earlier attempts, in which such modifications were done in a rather heuristic way [10,12], we use quantum mechanical perturbation theory to modify the quantum electron density  $n$  as

$$\tilde{n}(\phi) = \sum_l \tilde{N}_l(\phi - \phi_{\text{old}}) \left| \psi_l^{(k-1)} \right|^2, \quad (12)$$

$$\tilde{N}_l(\phi - \phi_{\text{old}}) = \left( \frac{2m_q k_B T}{\pi^2 \hbar^2} \right)^{1/2} \mathcal{F}_{-1/2} \left( \frac{E_F - E_l + e(\phi - \phi_{\text{old}})}{k_B T} \right). \quad (13)$$

Here,  $\tilde{n}(\phi)$  approximates the implicit dependence of  $n$  on the electrostatic potential  $\phi$  due to Schrödinger's equation, but yields the same numerical value as the original expression for  $n$  once  $\phi$  has converged.

In our original iteration approach we start by solving a modified Poisson equation containing  $\tilde{n}(\phi)$  as a predictor for  $n$

$$\nabla \cdot (\epsilon \nabla \phi) = -e \left[ -\tilde{n}(\phi) + p(\phi) + N_D^+(\phi) - N_A^-(\phi) \right] \quad (14)$$

to obtain the electrostatic potential  $\phi$ . This  $\phi$  together with the predicted electron density  $\tilde{n}$  is then used to determine the potentials within Schrödinger's equation (corrector)

$$-\frac{\hbar^2}{2} \nabla \cdot \left[ \frac{1}{m^*} \nabla \psi_l \right] + \left[ V_h - e\phi + V_{\text{xc}}(\tilde{n}) - E_l \right] \psi_l = 0 \quad (15)$$

to calculate a corrected update to the exact electron density. No further steps are necessary to insure convergence [13].

We compare the convergence speed of this predictor–corrector–type method with a fast adaptive underrelaxation scheme (an adaptive nonlinear version of the standard Gauss–Seidel algorithm), which uses a heuristic method to adjust the relaxation parameter  $\omega$  [7]. We find that for our predictor–corrector the residual decreases by almost one order of magnitude each step (Fig. 4), which is a 6-fold increase in

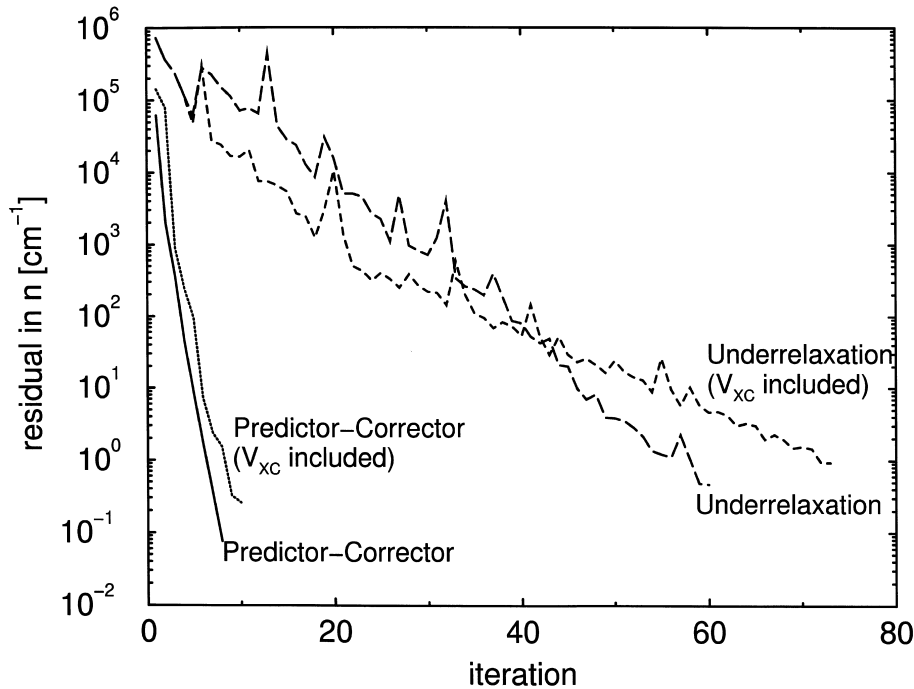


Fig. 4. The residual of the quantum electron density during the outer iteration for the GaAs-based device shown in Fig. 1. The gate voltages were chosen as  $V_g = 1.3$  V with respect to the substrate.

convergence speed compared to underrelaxation. Additionally we find that the residual decreases uniformly from one step to the next, while for the heuristic underrelaxation algorithm occasional increases are possible. The inclusion of exchange correlation  $V_{xc}(n)$  results in an additional slowdown of convergence for the underrelaxation scheme and also decreases its stability. However, our predictor–corrector method remains stable and similarly efficient.

There are practical situations when even the described predictor–corrector procedure may not converge completely or fail to converge at all. Invariably, these situations have in common the fact that there is a large number of occupied states in the system. This is the case of some undoped silicon quantum wire structures at room temperature (Fig. 6(b)). For such physical systems it is often impossible to calculate all occupied wavefunctions because of memory limitations, as outlined earlier. As a result, there is a certain amount of *missing quantum charge* caused by the exclusion from the calculation of quantum states corresponding to high order eigenvalues. As a result, the predictor  $\tilde{n}(\phi)$  becomes less accurate, and convergence problems can occur. Based on our experience, we can approximately state that the minimum obtainable residual in the outer iteration is in its order of magnitude comparable to the total amount of the missing quantum charge, since usually the inclusion of more states leads immediately to better convergence.

## 5. Applications

The first example examined here is a GaAs-based quantum structure. A schematic diagram of the geometry is shown in Fig. 1. The temperature of operation is 4.2 K. The convergence properties of the overall algorithm for this particular structure are shown in Figs. 3 and 4, and the corresponding distribution of eigenvalues for a voltage  $V_g = 1.3$  V on the gates is shown in Fig. 5. It is necessary to operate at cryogenic temperatures in order to isolate only a few states in the quantum region for device sizes which are practical

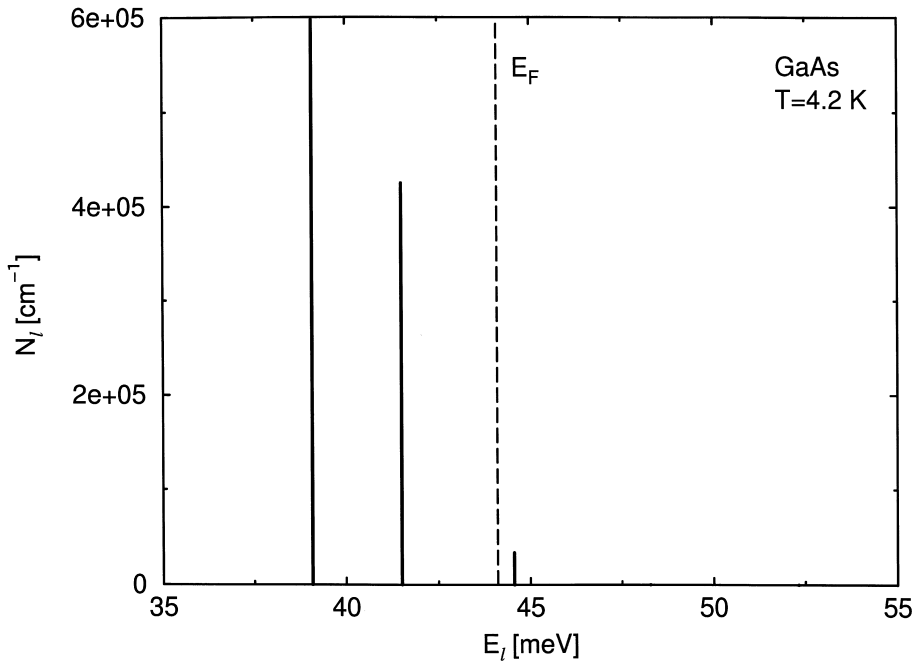


Fig. 5. Occupation numbers  $N_l$  of states  $E_l$  for the GaAs device shown in Fig. 1. The Fermi level  $E_F$  is indicated by the dashed line. All energies are normalized with respect to the bottom of the conduction band potential. The bias is  $V_g = 1.3$  V for both gates.

for fabrication. A similar state distribution at higher temperatures could be possible only if the distance between the gates could be reduced to 10 nm or so. The GaAs/AlGaAs system obtains electron population in the wire region through carrier transfer from the top highly doped layer (modulation doping). The role of the side gates is to confine interface charge within a narrow wire.

The use of a structure based on the Metal–Oxide–Semiconductor (MOS) silicon system allows one to obtain a quantum wire in a different way. The top layer of  $\text{SiO}_2$  is insulating and does not provide carriers, but the voltage on the gate attracts electrons to the surface from the semiconductor itself. Therefore, it is possible to form a wire by using one single gate contact. We were interested in exploring possible configurations for single gate silicon quantum wires and among various geometries tested, we found that the structure shown in Fig. 2 has very interesting properties. The top gate has a T-shape which may be embedded in an oxide trench, thus creating a potential well within the p-doped substrate. The size of the gate can be quite small, and therefore higher temperature operation becomes possible. We use in our calculation room temperature (300 K).

The small dimensions of this device allow one to consider in practice only a nearly undoped or a highly doped substrate. For intermediate dopant concentrations there would only be a few dopant atoms within the channel, leading to unacceptable statistical fluctuations of device characteristics due to the random location of dopant atoms. Therefore, we choose an acceptor concentration of either  $N_A = 10^{18} \text{ cm}^{-3}$  for a highly doped device or  $N_A = 10^{10} \text{ cm}^{-3}$  for a nominally undoped one, where the latter concentration is a typical value for residual impurity concentration in undoped silicon. We do not concern ourselves with random fluctuation of such impurities here, but for practical circuit applications where repeatability of device properties over many structures should be assured, control of random fluctuation of impurity in the path of the quantum wire is an important issue. In all the simulations for silicon wires we assume a typical surface charge density of  $4 \times 10^{10} \text{ cm}^{-2}$  at the silicon oxide interface.

The occupation numbers  $N_l$  of the states  $E_l$  belonging to the first eigenvalue ladder at a total occupation of  $\int n \, dx = 3.9 \times 10^6 \text{ cm}^{-1}$ , for the configuration depicted in Fig. 2, are given in Fig. 6. Unlike low temperature devices, which feature a sharp transition in the occupation of quantum states around the Fermi level  $E_F$  towards higher energies, we see for room temperature devices a slow exponential decay of occupation numbers. The reason for this behavior is that almost all energy levels are located above  $E_F$ , where the

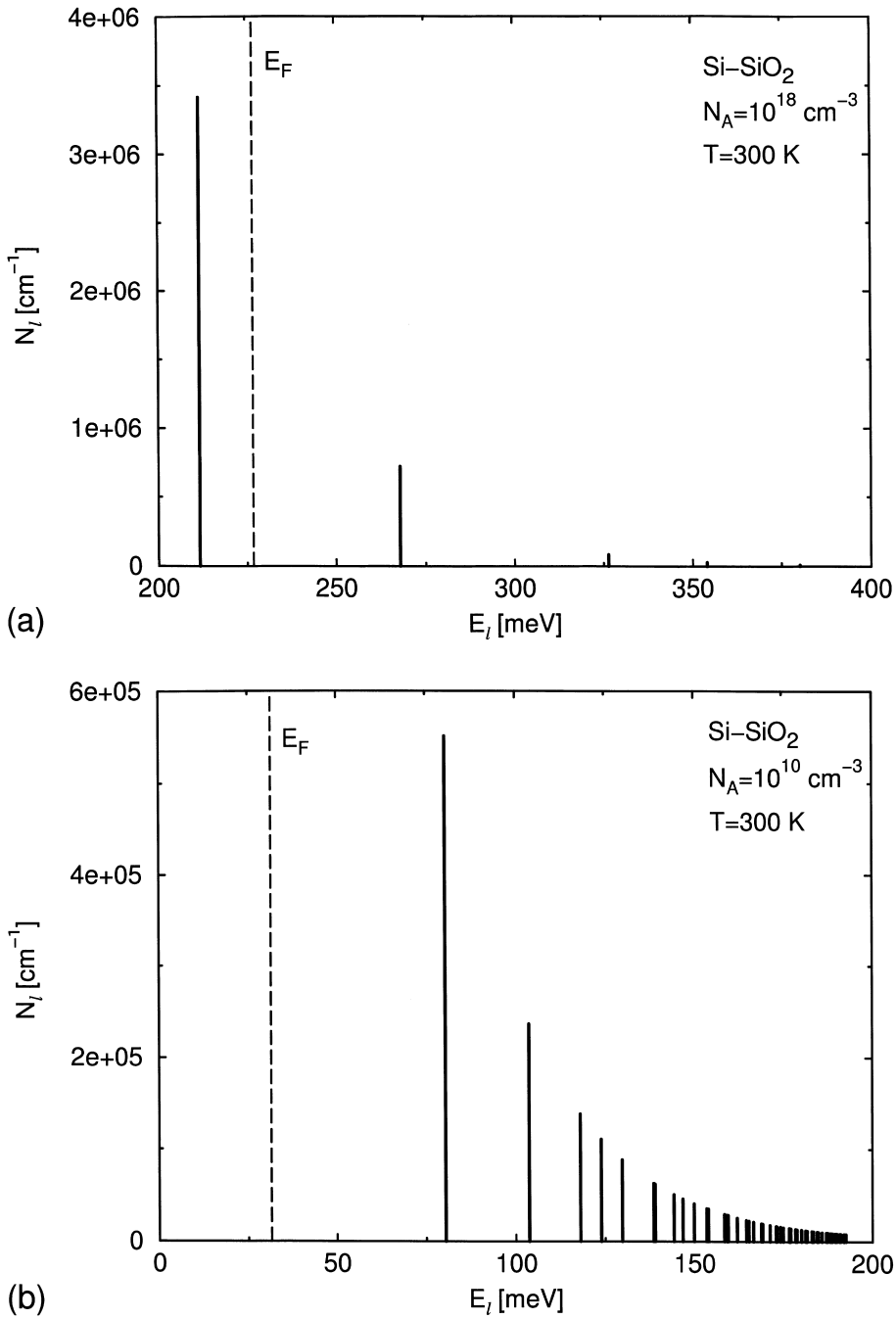


Fig. 6. Occupation numbers  $N_i$  of states  $E_i$  for the T-gate device shown in Fig. 2. The Fermi level  $E_F$  is indicated by the dashed line. All energies are normalized with respect to the bottom of the conduction band potential. Only the states belonging to the first valley are shown. The total integrated electron density is  $3.9 \times 10^6 \text{ cm}^{-1}$  in both cases, and the gate bias is 2.5 V for the highly doped (a) and 0.8 V for the undoped device (b).

distribution function describing their occupations  $\mathcal{F}_{-1/2}$  decays exponentially with a decay constant  $K_B T = 25 \text{ meV}$ .

We find, however, that for the same total charge inside of the quantum wire  $\int n \, dx = 3.9 \times 10^6 \text{ cm}^{-1}$  the number of occupied energy levels is quite different for the highly doped and the undoped device. While for the highly doped structure only a few states are occupied and most of the electrons are concentrated in the

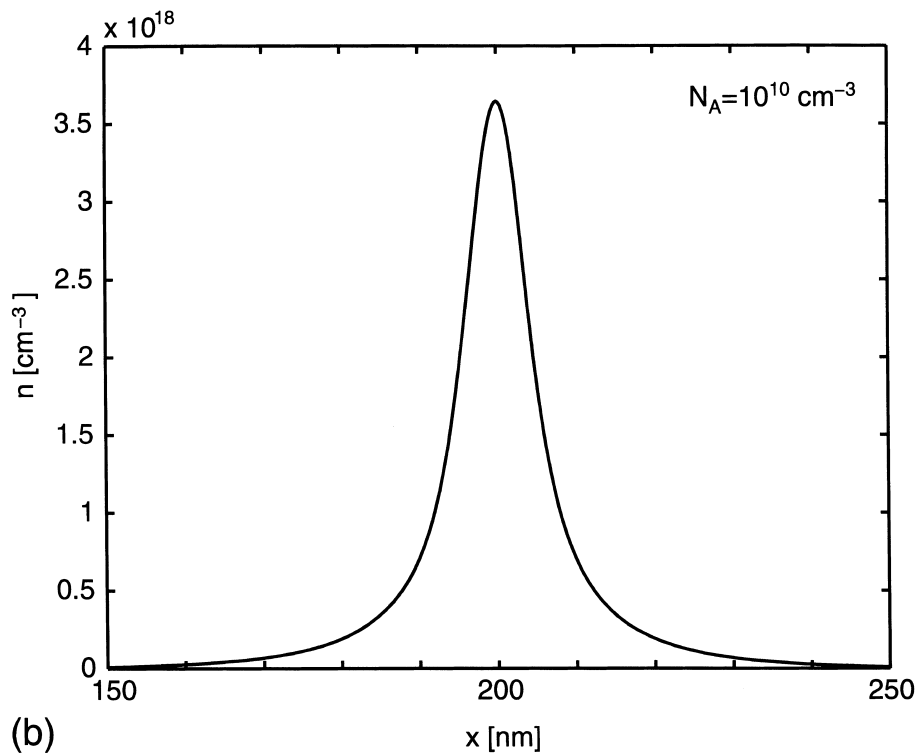
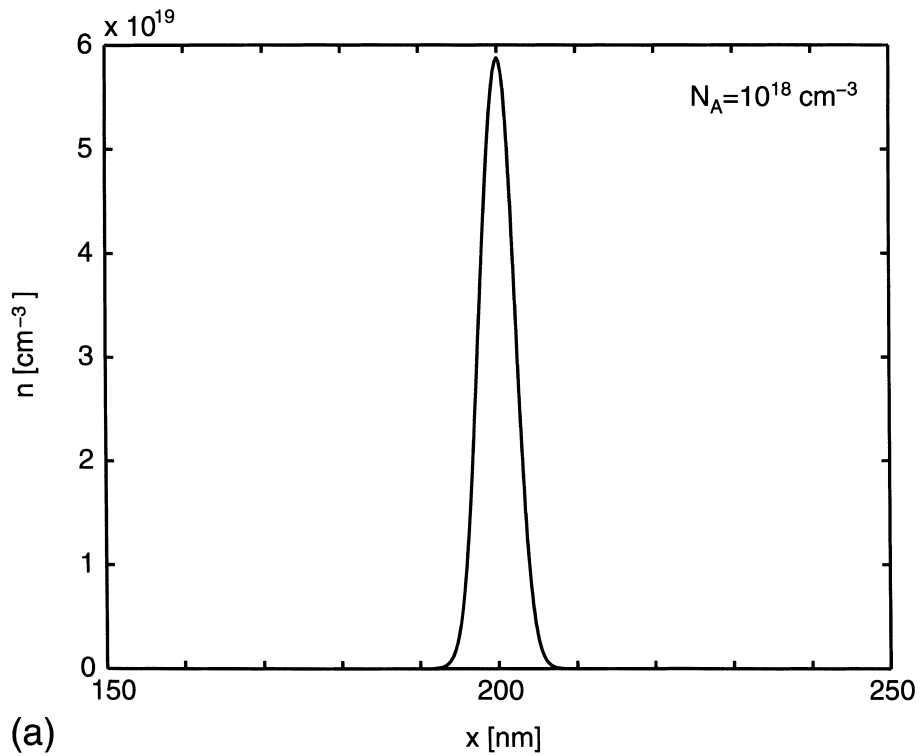


Fig. 7. Cross-sections of the quantum electron density  $n$  parallel to the Si–SiO<sub>2</sub> interface corresponding to the spectra shown in Fig. 6. Both sections cut through the maximum of the electron density (the distance to the interface is 0.9 nm for the highly doped (a) and 1.6 nm for the undoped case (b)). The gate is located at  $x = 200$  nm.

ground state of the system (Fig. 6(a)), there is a dense spectrum of occupied states for the undoped case (Fig. 6(b)).

We can understand this difference by examining the cross-sections of the electron density  $n$  parallel to the Si–SiO<sub>2</sub> interface. We find that in the highly doped device the quantum wire is very compact (Fig. 7(a)) with a width of about 20 nm and a core density of  $6 \times 10^{19} \text{ cm}^{-3}$ , and for such tight confinement size quantization results in a large separation between energy levels. In fact, most of the electrons occupy only the lowest energy state of the first conduction band valley (Table 2), and the quantum wire has quasi-mono-mode behavior. Therefore, for this specific device it might be possible to observe quantum effects even at room temperature, according to the theoretical calculation.

On the other hand, the wire in the undoped device is much wider (Fig. 7(b)) with spread of the electron density on the sides extending over a distance of more than 60 nm, and the core density is only  $4 \times 10^{18} \text{ cm}^{-3}$ , resulting in a much denser spectrum. This dense spectrum should prevent any observation of quantum effects and result in a more classical behavior of the transport.

The width of the undoped wire is strongly influenced by the shape of the gate. If the top of the T-shaped gate is widened, for example by metalization of the whole SiO<sub>2</sub> surface similar to the device described in [14], we found that a two-dimensional charge sheet forms at the silicon-oxide interface, which completely surrounds the quantum wire. This charge sheet persists even at gate voltages far below threshold, making it extremely difficult to realize adjacent wires that can be electrically insulated from each other.

Finally, let us examine for both doping cases the dependence of the electron density on the gate voltage. Fig. 8 shows the integrated electron density in the quantum wire and in the substrate as a function of the gate potential (referenced to the condition of flat band potential). We notice that for the highly doped device the channel is turned on at much higher voltage. The plots suggest a “threshold” of approximately 2.0 V for the highly doped structure (Fig. 8(a)) and 0.5 V for the undoped one (Fig. 8(b)). The undoped system would appear to be more suitable for low bias operation. However, one should keep in mind that, as shown in Fig. 8(b), there is a considerable total electron charge in the substrate outside of the quantum wire (scaled to same units as the quantum wire charge in the plot, for comparison). This suggests that it would be difficult to switch off completely the conduction in the structure. One should probably consider a Silicon-on-insulator (SOI) structure or a highly doped p-type ground plane to improve control, reducing the undoped silicon top layer to 100 nm or less. This arrangement reduces the number of carriers available outside of the wire region and is therefore expected to reduce the sub-threshold current, thus improving the switching behavior of the structure.

Table 2

The most occupied states for the highly doped T-gate device. The total charge in the quantum wire is  $3.9 \times 10^6 \text{ cm}^{-1}$  at a gate bias of 2.5 V

Ladder	State	Energy (meV)	Occupation number ( $\text{cm}^{-1}$ )
1	1	208	2 881 414
1	2	267	487 843
1	3	328	50 291
1	4	349	22 294
1	5	383	5 987
2	1	299	149 144
2	2	322	62 758
2	3	347	24 186
2	4	372	9 210
2	5	396	3 562
3	1	314	192 589
3	2	368	23 829
3	3	424	2 765
3	4	476	377
3	5	523	60

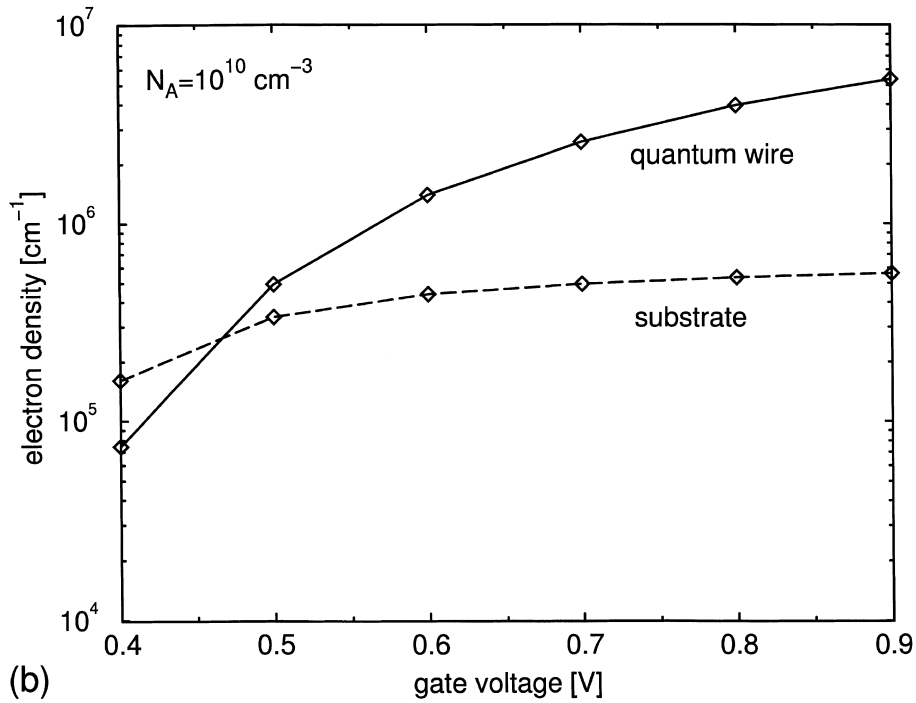
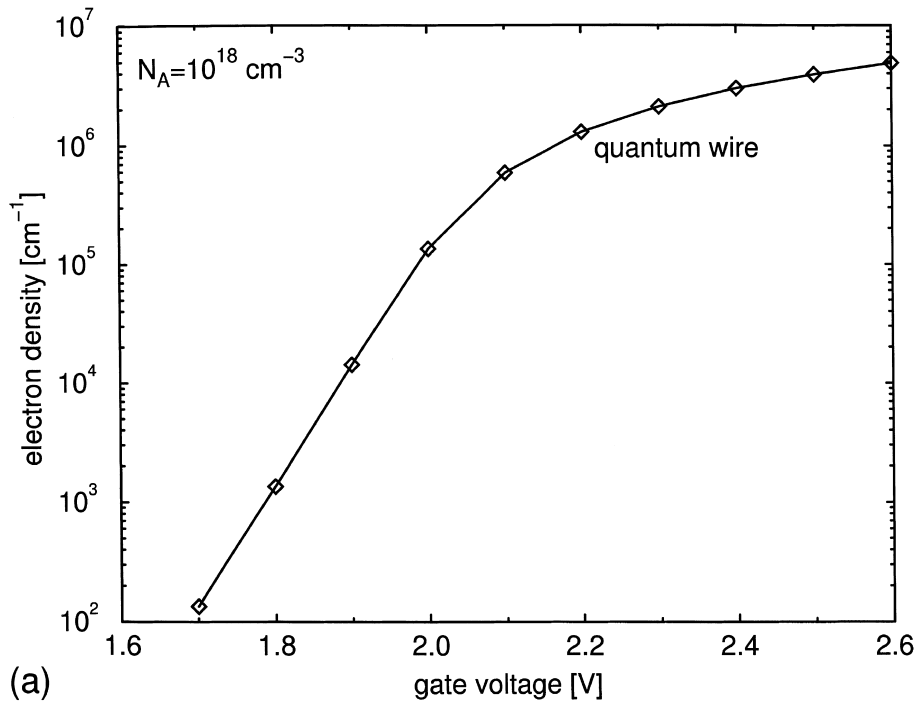


Fig. 8. The integrated electron density in the quantum wire and in the substrate (undoped case only) as function of the gate potential. All potentials are normalized against the flat-band condition.

## 6. Conclusions

Computer simulation of nanoscale semiconductor structures provides a way to probe microscopic behavior of electronic quantum states over a wide parameter space. Although the simulated structures are necessarily idealized, the numerical results are very valuable to point out the configurations that are more promising for practical realization. The examples presented here show, for instance, that in principle it is possible to realize silicon quantum wire structures at room temperature, with states sufficiently close to monomode condition. Quantum transport effects could be observable if such structures are fabricated.

The computations have been performed on Hewlett–Packard C-110 workstations. The mesh sizes employed were  $90 \times 100$  lines for the GaAs geometry and  $130 \times 130$  lines for the silicon based devices, resulting into simulation run-times of about 10 min for the GaAs structure, 30 min for the highly doped silicon device, and several hours for the undoped silicon system.

## Acknowledgements

This work was supported by the National Science Foundation grants ECS 95-09751, a Nato Collaborative Grant CRG.950753, and by a graduate fellowship (A.T.) of the CSE program at the University of Illinois.

## References

- [1] G.H. Golub, C.F. Van Loan, *Matrix Computations*, John Hopkins University Press, Baltimore, MD, 1996.
- [2] T. Dupont, R.P. Kendall, H.H. Rachford, An approximate factorization procedure for solving self-adjoint elliptic difference equations, *SIAM J. Numer. Anal.* 5 (1968) 559–573.
- [3] R. Chandra, *Conjugate gradient methods for partial differential equations*, Ph.D. Thesis, Yale University, 1978.
- [4] T. Kerkhoven, M.W. Raschke, U. Ravaoli, Self-consistent simulation of quantum wires in periodic heterojunction structures, *J. Appl. Phys.* 74 (1993) 1199–1204.
- [5] H.M. Antia, Rational function approximations for Fermi–Dirac integrals, *Astrophys. J. Supp. Ser.* 84 (1993) 101–108.
- [6] A. Trellakis, A.T. Galick, U. Ravaoli, Rational Chebyshev approximation for the Fermi–Dirac integral  $\mathcal{F}_{-3/2}(x)$ , *Solid-State Electron* 41 (1997) 771–773.
- [7] A.T. Galick, *Efficient solution of large sparse eigenvalue problems in microelectronic simulation*, Ph.D. Thesis, University of Illinois at Urbana-Champaign, 1993.
- [8] A.T. Galick, T. Kerkhoven, U. Ravaoli, Iterative solution of the eigenvalue problem for a dielectric waveguide, *IEEE Trans. Microwave Theory and Techniques* 40 (1992) 699–705.
- [9] Y. Saad, *Numerical Methods for Large Eigenvalue Problems*, Manchester University Press, Manchester, 1992.
- [10] S.E. Laux, Numerical methods for calculating self-consistent solutions of electron states in narrow channels, in: J.J.H. Miller (Ed.), *Proceedings of the Fifth International NASECODE Conference*, Boole Press, Dublin, Ireland, 1987, pp. 270–275.
- [11] T. Kerkhoven, A.T. Galick, U. Ravaoli, J.H. Ahrends, Y. Saad, Efficient numerical simulation of electron states in quantum wires, *J. Appl. Phys.* 68 (1990) 3461–3469.
- [12] A. Pacelli, Self-consistent solution of the Schrödinger equation in quantum wells by implicit iteration, *IEEE Trans. Electron Devices* 44 (1997) 1169–1171.
- [13] A. Trellakis, A.T. Galick, A. Pacelli, U. Ravaoli, Iteration scheme for the solution of the two-dimensional Schrödinger–Poisson equations in quantum structures, *J. Appl. Phys.* 81 (1997) 7880–7884.
- [14] T. Tsukui, S. Oda, Computer simulation and measurement of capacitance–voltage characteristics in quantum wire devices of trench-oxide MOS structure, *Jpn. J. Appl. Phys.* 34 (1995) 874–877.